Fourier-space TEM reconstructions with symmetry adapted functions for all rotational point groups

Stefano Trapani, Jorge Navaza

Fourier-space TEM reconstructions with symmetry adapted functions for all rotational point groups.

Stefano Trapani[a,b,c,d,*], Jorge Navaza[e,f,g,h]

[a] *Centre de Biochimie Structurale, Université Montpellier 2, 29 rue de Navacelles, 34090 Montpellier, France.*
[b] *Centre de Biochimie Structurale, Université Montpellier 1, 29 rue de Navacelles, 34090 Montpellier, France.*
[c] *Centre de Biochimie Structurale, CNRS, UMR 5048, 29 rue de Navacelles, 34090 Montpellier, France.*
[d] *Centre de Biochimie Structurale, INSERM, UMR 1054, 29 rue de Navacelles, 34090 Montpellier, France.*
[e] *Unidad de Biofísica, CSIC-UPV/EHU, Barrio Sarriena S/N, 48940 Leioa, Bizkaia, Spain.*
[f] *Institut de Biologie Structurale Jean-Pierre Ebel, CNRS, UMR 5075, 41 rue Jules Horowitz, F-38027 Grenoble, France.*
[g] *Institut de Biologie Structurale Jean-Pierre Ebel, CEA, UMR 5075, 41 rue Jules Horowitz, F-38027 Grenoble, France.*
[h] *Institut de Biologie Structurale Jean-Pierre Ebel, Univ. Joseph Fourier Grenoble 1, UMR 5075, 41 rue Jules Horowitz, F-38027 Grenoble, France.*

Abstract

A general-purpose and simple expression for the coefficients of symmetry adapted functions referred to conveniently oriented symmetry axes is given for all rotational point groups. The expression involves the computation of reduced Wigner-matrix elements corresponding to an angle specific to each group and has the computational advantage of leading to Fourier-space TEM (transmission electron microscopy) reconstruction procedures involving only real valued unknowns. Using this expression, a protocol for *ab-initio* view and center assignment and reconstruction so far used for icosahedral parti-

*corresponding author
Email address: stefano.trapani@cbs.fr (Stefano Trapani)
URL: http://www.cbs.fr (Stefano Trapani)

cles has been tested with experimental data in other point groups.

Keywords: symmetry adapted function, TEM reconstruction, point group

1. Introduction

The use of spherical harmonics in single particle transmission electron microscopy (TEM) was first proposed and implemented by Provencher and Vogel (1988). In their formulation the scattering density was expanded in a complete set of orthonormal functions, products of spherical harmonics with conveniently chosen radial functions, in general eigenfunctions of a differential equation problem. When the isolated particle displays some point-group symmetry, its scattering density can be conveniently described in terms of symmetry adapted functions (SAF), i.e. linear combinations of spherical harmonics that satisfy the symmetry of the object. The three dimensional (3D) reconstruction of particles using SAFs associated to the icosahedral symmetry group was thoroughly analyzed (Navaza, 2003). The angular part of the Fourier transform of the scattering density was expanded in terms of SAFs and the radial part —the unknown functions in the reconstruction procedure— were determined from the Fourier-Bessel transforms of the particle's projections. A particularly simple expression for the SAF coefficients, based on the reduced projection operator formalism of Fan et al. (1999), was used.

The derivation of formulas for SAFs and issues related to their practical implementations have been the subject of a number of publications, especially in the field of molecular quantum mechanics (see for example: Prandl et al. (1996); Blanco et al. (1997); Fan et al. (1999); Schmidt and Žďánská (2000)). More recently Liu et al. (2008) and Zeng et al. (2010) implemented

a reconstruction technique based on icosahedral and octahedral SAFs, following the method of Prandl et al. (1996) and Schmidt and Žďánská (2000). Although the mathematics have been developed in full detail, simple and efficient algorithms for computing high order SAFs are still necessary. In the present article we have extended Fan's expression to all rotational groups. For the icosahedral and cubic groups the formula involves the computation of rows of the reduced Wigner-matrices with one definite angle for each group, which are calculated on the fly by using a two-terms recursive formula. For the C_n groups the SAFs split into two sets of orthogonal functions. One of these sets presents two alternatives: one may choose real valued SAF coefficients and purely imaginary radial functions of the Fourier transform, or conversely. In TEM reconstructions the latter is preferable as the most demanding calculations in CPU time involve radial functions.

To our knowledge, SAF-based TEM reconstructions were compared with results obtained by other methods only in few cases, all involving icosahedral symmetry: reconstructions given the views (Liu et al., 2008) and the whole process of view and center assignment and reconstruction (Estrozi and Navaza, 2010). In both cases there was an improvement in resolution of about 1Å as measured by the Fourier shell correlation. Although efficient for reconstructions, SAFs proved to be particularly suitable for views and centers assignment when used with the fast rotation matching technique (Kovacs and Wriggers, 2002; Estrozi and Navaza, 2008). Indeed, in the Rotavirus DLP reconstruction, which took about 14 months of CPU time, not only views and centers were more accurately determined but also there was a substantial gain in time (Estrozi and Navaza, 2010).

For lower symmetries the number of unknown functions to be determined increases, as well as the computer effort. Moreover, view determi-

nation based on a single image (Navaza, 2003) will no longer be possible for all symmetry groups. Nevertheless, the *ab-initio* view and center assignment and the reconstruction protocol described in Navaza (2003) has been successfully applied to experimental data obtained from tetrahedral and D_7 symmetric particles.

2. Symmetry in Fourier-space TEM reconstructions

The aim of TEM reconstructions is to obtain the 3D scattering density starting from its two-dimensional (2D) projections. The problem can be formulated in Fourier (reciprocal) space as, according to the so called "projection theorem", the Fourier transform of a projection corresponds to the central section perpendicular to the projection direction, of the scattering density Fourier transform. The 3D Fourier transform can thus be recovered from its central sections, either by interpolation or by assuming a functional form that depends on a certain number of parameters to be determined by an optimization procedure. It is crucial to incorporate as much as possible pertinent information into this functional form, both to reduce the number of parameters to be determined and to enforce redundancy in the optimization procedure.

One important piece of information is symmetry. For isolated objects of biological origin the only possible symmetries are point groups consisting of a finite number of rotations (groups C_n, D_n, T, O and I in Schoenflies notation). Perhaps the most efficient way to deal with this kind of information is to use symmetry adapted functions invariant with respect to the group transformations.

2.1. Fourier coefficients in terms of SAFs

If $\mathbf{s}$ is the reciprocal vector with spherical coordinates (s, ϑ, φ) in a given reference frame, the general expression of a SAF is:

$$\mathcal{S}_{\mu}^{\ell}(\mathbf{s}/s) = \sum_{m=-\ell}^{\ell} A_{\mu,\,m}^{\ell}\,(-i)^{\ell}\,Y_{m}^{\ell}(\mathbf{s}/s)\;, \tag{1}$$

where $Y_{m}^{\ell}(\mathbf{s}/s) \equiv Y_{m}^{\ell}(\vartheta, \varphi)$ are the spherical harmonics of degree ℓ and order m (see definition in Landau and Lifschitz (1967)), and $A_{\mu,\,m}^{\ell}$ are the coefficients of the SAF of degree ℓ and label μ. Their values depend on the orientation of the symmetry axes with respect to the reference frame. We note that SAFs involve only angular variables.

SAFs of different degrees are automatically orthogonal because of properties of the spherical harmonics. Otherwise, orthonormality is related to properties of the $A_{\mu,\,m}^{\ell}$ coefficients. It must be noted that in most applications the functions $\mathcal{S}_{\mu}^{\ell}(\mathbf{s}/s)$ need only to be independent. For this, the matrix of inner products, the Gram matrix

$$\int \overline{\mathcal{S}_{\mu'}^{\ell}(\mathbf{s}/s)}\,\mathcal{S}_{\mu}^{\ell}(\mathbf{s}/s)\,d^{\,2}\mathbf{s} = \sum_{m=-\ell}^{\ell} \overline{A_{\mu',\,m}^{\ell}}\,A_{\mu,\,m}^{\ell}\;, \tag{2}$$

must be non-singular.

In terms of independent SAFs, the 3D Fourier coefficients $\mathcal{F}$ of the particle scattering density take the form

$$\mathcal{F}(\mathbf{s}) = \sum_{\ell=0}^{\ell_{\max}} \sum_{\mu=1}^{n_{\ell}} F_{\mu}^{\ell}(s)\,\mathcal{S}_{\mu}^{\ell}(\mathbf{s}/s)\;. \tag{3}$$

The particle radial functions $F_{\mu}^{\ell}(s)$ are the unknowns to be determined by the reconstruction procedure (see section 3). For each degree ℓ the inner summation extends over the independent SAFs, whose number, denoted n_{ℓ}, is called the multiplicity. It is understood that ℓ's with $n_{\ell} = 0$ are excluded

from the summation. The maximum degree ℓ included in Eqn.3 is related to the particle's diameter and to resolution by $\ell_{\max} \approx \pi\,\text{diameter}/\text{resolution}$.

A most important property of the Fourier coefficients is hermiticity, $\overline{\mathcal{F}^{\ell}_{\mu}(\mathbf{s})} = \mathcal{F}^{\ell}_{\mu}(-\mathbf{s})$ (the bar over the symbol denotes complex conjugation), stemming from the fact that the scattering density is a real valued function. Taking into account that $\overline{Y^{\ell}_{m}(-\mathbf{s}/s)} = (-1)^m\, Y^{\ell}_{-m}(\mathbf{s}/s)$, it follows that SAFs will also be hermitian functions if the coefficients satisfy

$$\overline{A^{\ell}_{\mu,\,m}} = (-1)^{\ell-m}\, A^{\ell}_{\mu,\,-m}\ . \tag{4}$$

Consequently, the radial functions $F^{\ell}_{\mu}(s)$ will be real valued, which is an advantage, computation-wise. We will show that the orientation of the symmetry axes can be chosen so that Eqn.4 holds for all rotational point groups.

2.2. The SAF coefficients formula

The values of the SAF coefficients depend on the orientation of the symmetry axes with respect to an orthonormal $\{\mathbf{X}, \mathbf{Y}, \mathbf{Z}\}$ reference frame. The coefficients may be obtained from the projector $\mathcal{P}^{\ell}$ of the totally symmetric representation of the point group within the ℓ^{th} representation of the rotation group. By orienting the axes as described in Table 1, the projector is given by the following expression, valid for all finite rotational groups:

$$\begin{aligned}\mathcal{P}^{\ell}_{m',\,m} = \frac{1}{U}\Big\{&\Big[\delta_{\,m',m} + W\,(-1)^{m'/V}\, d^{\,\ell}_{\,m',m}(\Theta)\Big] \\ &+\ K(-1)^{\ell-m}\Big[\delta_{\,m',-m} + W\,(-1)^{m'/V}\, d^{\,\ell}_{\,m',-m}(\Theta)\Big]\Big\}\end{aligned} \tag{5}$$

if $(m' \bmod N) = (m \bmod N) = M$, and $\mathcal{P}^{\ell}_{m',\,m} = 0$ otherwise. The values of Θ, U, W, V, K, N and M are specific to each group (Table 1). The symbol $\delta_{\,m',m}$ is Kronecker's delta and $d^{\,\ell}_{\,m',\,m}$ are the reduced matrix elements of

the irreducible representations of the rotation group (the so called Wigner d-matrices, see definition in Brink and Satchler (1994)). Each row of the reduced matrix is obtained by using the recurrence relation (Navaza, 2001)

$$d^{\ell}_{m',m-1}(\Theta) = \sqrt{\frac{(\ell-m)(\ell+m+1)}{(\ell-m+1)(\ell+m)}}\, d^{\ell}_{m',m+1}(\Theta) - \frac{2\,[m' - m\,\cos(\Theta)]}{\sqrt{(\ell-m+1)(\ell+m)}\,\sin(\Theta)}\, d^{\ell}_{m',m}(\Theta)\;, \tag{6}$$

starting from the rightmost values

$$d^{\ell}_{m',\ell}(\Theta) = \sqrt{\frac{(2\ell)!}{(\ell-m')!(\ell+m')!}}\,\sin(\frac{\Theta}{2})^{\ell-m'}\,\cos(\frac{\Theta}{2})^{\ell+m'}\;. \tag{7}$$

The general-purpose projector (5) was obtained by using explicit expressions of the irreducible matrices of the rotation group; it coincides with Fan's result for the icosahedral group (Fan et al., 1999). For groups C_n and T the projector is the direct sum of two projectors ($\mathcal{P}1$ and $\mathcal{P}2$ in Table 1) acting on orthogonal subspaces. Projectors $\mathcal{P}1$ are equal to the projectors of the D_n and O groups (supergroups of C_n and T respectively). Projectors $\mathcal{P}2$ correspond to the A_2 irreducible representations of $D_{n>2}$ and O, and the B_1 irreducible representation of D_2.

We note that the projector (5) is real valued, symmetric : $\mathcal{P}^{\ell}_{m',m} = \mathcal{P}^{\ell}_{m,m'}$, and idempotent : $\mathcal{P}^{\ell}\,\mathcal{P}^{\ell} = \mathcal{P}^{\ell}$. From this last property it follows that the rows (or columns) of $\mathcal{P}^{\ell}$ can be chosen as SAF coefficients and that the Gram matrix (Eqn.2) of the functions so constructed is also $\mathcal{P}^{\ell}$. In particular, for nonzero diagonal elements of the projector,

$$A^{\ell}_{\nu,m} = \mathcal{P}^{\ell}_{\nu,m}/\sqrt{\mathcal{P}^{\ell}_{\nu,\nu}} \tag{8}$$

are normalized SAF coefficients, with labels $-\ell \le \nu \le \ell$, and satisfy $A^{\ell}_{\nu,m} = K\,(-1)^{\ell-m}\,A^{\ell}_{\nu,-m}$. They are not, in general, independent.

Hermiticity ($K = 1$) results from the invariance of the projection operators of groups D_n, T, O and I under multiplication by a twofold rotation around the $\mathbf{Y}$ axis. This same multiplication interchanges symmetry operations with opposite characters in the A_2 irreducible representation of $D_{n>2}$ and the B_1 representation of D_2, leading to the antihermiticity ($K = -1$) of the SAFs based on the $\mathcal{P}2$ projector of the C_n groups. For these functions hermiticity is recovered by redefining $A^{\ell}_{\nu,m} = i\,\mathcal{P}^{\ell}_{\nu,m}/\sqrt{\mathcal{P}^{\ell}_{\nu,\nu}}$.

2.3. The multiplicity of SAFs

The number of independent SAFs for a given ℓ, i.e. the multiplicity n_ℓ, is obtained by character theory (see for example Landau and Lifschitz (1967)). It is given by the expression

$$n_\ell = \frac{1}{G}\sum_{k=1}^{G}\frac{\sin[(2\ell+1)\Phi_k/2]}{\sin(\Phi_k/2)}\,, \tag{9}$$

where G is the number of elements of the group and Φ_k denotes the rotation angle corresponding to the k^{th} transformation of the group. The summation includes the identity transformation whose contribution is obtained by taking the limit $\Phi \to 0$, giving $G^{-1}(2\ell+1)$. For all other transformations Φ_k can be written as $2\pi p_k/q_k$, where q_k is the order of the symmetry axis and $1 \le p_k < q_k$ is an integer.

The multiplicity may be written as a sum over axes orders. If N_q denotes the number of axes of order $q > 1$, then

$$\begin{aligned} n_\ell &= \frac{1}{G}\left[2\ell+1+\sum_q N_q \sum_{p=1}^{q-1}\frac{\sin[(2\ell+1)\pi p/q]}{\sin(\pi/q)}\right] \\ &= 1+\left[\ell-\sum_q N_q(\ell \bmod q)\right]2/G\,. \end{aligned} \tag{10}$$

It follows that if η denotes the least common multiple of all orders q, then the multiplicity increases by

$$\Delta = n_{\ell+\eta} - n_\ell = 2\eta/G \tag{11}$$

when ℓ increases by η. Expressions of n_ℓ, η and Δ for the different point groups are reported in Table 2. The values therein refer to the complete set of independent SAFs. For groups C_n and T the number of independent functions based on the projectors $\mathcal{P}1$ and $\mathcal{P}2$ are given in Table 3.

No elegant method was found to choose n_ℓ independent $A^\ell_{\nu,m}$ out of the $2\ell+1$ coefficients defined by Eqn.8 (but see Prandl et al. (1996), Zheng and Doerschuk (2000), Schmidt and Žďánská (2000)). However, we demonstrated numerically that the label ν can be chosen sequentially according to the rule

$$\nu = M + N[\mathrm{int}(\ell/N) + 1 - \mu] \qquad \text{for} \quad \mu = 1, \cdots, n_\ell \,. \tag{12}$$

For groups C_n and T the values of n_ℓ are those from Table 3. The $\mathcal{S}^\ell_\mu$ functions thus defined are orthogonal only for the C_n and D_n groups. For the other groups (T, O, I) we verified —by using high precision representations of numbers (Mathematica®, Wolfram Research, Inc., Champaign, IL)— that the associated Gram matrices are non-singular up to high degrees of the spherical harmonics representation ($\ell \leq 900$). For normal (64-bit) precision calculations, analysis of the Gram matrix eigenvalues shows (Table 4) that Eqn.12 is quite usable up to degree $\ell \simeq 221$ (cubic groups) and $\ell \simeq 644$ (icosahedral group).

3. Reconstruction procedures

The images on a transmission electron micrograph are related to the orthogonal projections of the particle scattering density. According to the projection theorem, the 2D Fourier transform of a projection is a central section of the 3D Fourier transform of the scattering density. It can be written as $\mathcal{F}(\mathbf{R}\,\mathbf{q})$, where $\mathbf{q}$ denotes a reciprocal vector lying on the equatorial plane, with spherical coordinates $(q, \pi/2, \varphi)$, and $\mathbf{R}$ is the rotation of the reference system that defines the view direction and the in-plane rotation associated to the projection. Thus, projections generate samples of the 3D Fourier transform. If $\mathcal{G}_k(\mathbf{q})$ denotes the 2D Fourier transform of the k^{th} projection associated to the orientation $\mathbf{R}_k$, then

$$\mathcal{G}_k(\mathbf{q}) = \mathcal{F}(\mathbf{R}_k\mathbf{q}) = \sum_{\ell=0}^{\ell_{\max}} \sum_{\mu=1}^{n_\ell} F_\mu^\ell(q)\, \mathcal{S}_\mu^\ell(\mathbf{R}_k\mathbf{q}/q) \; . \tag{13}$$

After view and center assignment, the image is identified with a projection and the left-hand term in Eqn.13 is replaced by the experimentally determined $\mathcal{G}_k(\mathbf{q})$. The radial functions $F_\mu^\ell(q)$ are the same for all images; they are determined by an optimization procedure, typically least-squares:

$$\sum_k \int \left| \mathcal{G}_k(\mathbf{q}) - \sum_{\ell=0}^{\ell_{\max}} \sum_{\mu=1}^{n_\ell} F_\mu^\ell(q)\, \mathcal{S}_\mu^\ell(\mathbf{R}_k\mathbf{q}/q) \right|^2 d^2\mathbf{q} \; . \tag{14}$$

This is Liu et al. (2008) and Zeng et al. (2010) reconstruction procedure.

For single image view assignment and fast projection matching (Navaza (2003); Estrozi and Navaza (2008)) Eqn.13 requires some modifications. When written in spherical coordinates and using the transformation formula of spherical harmonics

$$Y_m^\ell(\mathbf{R}\,\mathbf{s}/s) = \sum_{m'=-\ell}^{\ell} D_{m,m'}^\ell(\mathbf{R})\, Y_{m'}^\ell(\mathbf{s}/s) \; , \tag{15}$$

where $D^{\ell}_{m,m'}$ are the Wigner D-matrix elements (see definition in Brink and Satchler (1994)), Eqn.13 becomes

$$\mathcal{G}_k(q,\varphi) = \sum_{\ell=0}^{\ell_{\max}} \sum_{\mu=1}^{n_\ell} F^{\ell}_{\mu}(q) \sum_{m,m'=-\ell}^{\ell} A^{\ell}_{\mu,m'} D^{\ell}_{m',m}(\mathbf{R}_k)(-i)^{\ell} Y^{\ell}_{m}(\frac{\pi}{2},\varphi). \tag{16}$$

Calling, for short,

$$T^{\ell}_{\mu,m}(\mathbf{R}) = \sum_{m'=-\ell}^{\ell} A^{\ell}_{\mu,m'}\, D^{\ell}_{m',m}(\mathbf{R})\,(-i)^{\ell}\, Y^{\ell}_{m}(\pi/2,0)\ , \tag{17}$$

and performing a Fourier transformation on the φ angle,

$$G^{(k)}_{m}(q) = (2\pi)^{-1} \int \mathcal{G}_k(q,\varphi)\, \exp(-im\varphi)\, d\varphi\ , \tag{18}$$

the least-squares expression becomes

$$\sum_{k} \int \left| G^{(k)}_{m}(q) - \sum_{\ell=|m|}^{\ell_{\max}} \sum_{\mu=1}^{n_\ell} F^{\ell}_{\mu}(q)\, T^{\ell}_{\mu,m}(\mathbf{R}_k) \right|^2 q\, dq\ , \tag{19}$$

leading to the normal equation

$$\sum_{\ell',\mu'} \left[\sum_{k} \sum_{m} \overline{T^{\ell}_{\mu,m}(\mathbf{R}_k)}\, T^{\ell'}_{\mu',m}(\mathbf{R}_k) \right] F^{\ell'}_{\mu'}(q) = \\ = \sum_{k} \sum_{m} \overline{T^{\ell}_{\mu,m}(\mathbf{R}_k)}\, G^{(k)}_{m}(q)\ . \tag{20}$$

The $G^{(k)}_{m}(q)$ are implicit functions of the image center.

Eqn.20 may be used for different tasks: (i) to obtain an estimate of individual centers and orientations; (ii) to obtain an estimate of individual centers and orientations using the information of the already determined ones; (iii) to determine the radial functions based on any number of centered and oriented images which, after substitution into Eqn.3, give the

Fourier coefficients of the scattering density. All these tasks were implemented, for icosahedral symmetry, in the RIco program (Navaza, 2003). They are usually performed at low resolution using a limited number of images. However, to attain high resolution several thousands of TEM images are required and calculations become extremely long. Then, the low resolution radial functions determined with RIco are used by the fast projection matching program FPM (Estrozi and Navaza, 2008) to assign views and centers to the remaining images. New radial functions are thus determined at higher resolution by task (iii). The iteration of the last two steps was used by Estrozi and Navaza (2010) to obtain a high resolution 3D reconstruction of Rotavirus double-layered particles.

3.1. Resolution issues

The radial functions $G_m^{(k)}(q)$ are the Fourier-Bessel transforms of the images. They are calculated by numerical integration of the expression

$$G_m^{(k)}(q) = \\ i^m \int_0^{\text{radius}} \left[\int_0^{2\pi} \mathcal{I}^{(k)}(u,\phi) \exp(-im\phi) d\phi \right] J_m(2\pi q u) u \, du, \qquad (21)$$

where $\mathcal{I}^{(k)}(u,\phi)$ is the k^{th} image, (u,ϕ) are the polar coordinates of a direct space vector on the image plane, and J_m is the Bessel function of integer order m. A similar expression holds for the particle radial functions $F_\mu^\ell(s)$ in terms of the spherical Bessel functions j_ℓ. A general property of Bessel functions is that J_m and j_ℓ start taking appreciable values for arguments of the order of m and ℓ, respectively, as illustrated in Fig 1. Thus, the highest argument of the Bessel functions determines the highest angular orders m and ℓ entering in the preceding formulas. A sensible approximation

is $\ell_{\max} \approx \arg_{\max} = 2\pi$ radius $q_{\max}$, as stated in section 2.1 . Note that $\ell_{\max}$ is only the upper limit of the angular components for a given resolution.

In practice $\ell_{\max}$ is chosen so that the normal matrix in Eqn.20 is well conditioned; this is controlled by the ratio between the extreme eigenvalues. It must be noted that the normal matrix does not depend on data or resolution; it depends only on view directions (α and β angles in the Euler parameterization of $\mathbf{R}$). However, Eqn.20 can only be used for $q \leq q_{\max}$. Indeed, beyond this resolution $G_m^{(k)}(q)$ with angular components $m > \ell_{\max}$ also contribute to $F_\mu^\ell(q)$. As a consequence the different tasks in RIco are accomplished at different resolutions. The *ab-initio* individual image view assignment requires relatively small $\ell_{\max}$ whereas, when several images are simultaneously considered, Eqn.20 is in general well conditioned with high $\ell_{\max}$ so that high resolution particle radial functions can be determined. Albeit the actual resolution of the final reconstruction must be assessed by other methods (for example Fourier Shell Correlation), as with other reconstruction techniques.

4. Examples

The general-purpose SAF expression was introduced into the program RIco and applied to two sets of experimental data. One of them corresponds to negatively stained DHQ (Trapani et al., 2010), a 195 kDa protein displaying tetrahedral symmetry, and the other corresponds to cryo-EM images of GroEl (Vossman, 2008), a protein complex displaying D_7 symmetry. For DHQ we used 100 images boxed with the help of the X3D program (Conway and Steven, 1999) and for GroEl we used 70 images boxed with a program developped by Jon Agirre. The resolutions used in the calculations

were 15Å for DHQ and 20Å for GroEL, and the maximum degree of the spherical harmonics was $\ell_{\max} = 30$. Although the calculations aimed only at producing a low resolution starting model, the reconstructions (Figure 2 and 3) already displayed the characteristic features of the structures.

5. Conclusions

Inspired by the work of Fan et al. (1999) a simple and general expression was found for the SAF coefficients of the totally symmetric representations of the rotational point groups, which has the numerical advantage of being hermitian. The coefficients are real valued excepting for a subset of SAFs of the C_n groups, where they are purely imaginary. For the groups T, O and I, the expression requires, for each degree ℓ, n_ℓ rows from a single reduced Wigner-matrix, which are calculated on the fly by using a very stable and fast recursive algorithm.

The problem of the multiplicity of the representations was analyzed numerically. By using a high precision representation of numbers we were able to demonstrate that the Gram matrix of the normalized SAFs obtained by the rule (12) is non singular at least up to $\ell = 900$, so that a Gram-Schmidt orthogonalization may be performed, if necessary. However, the simple rule provides quite usable SAFs for $\ell \leq 221$ with groups T and O and $\ell \leq 644$ for the icosahedral group.

The general SAF expression keeps the original simple form derived by Fan et al. (1999). Thus, it was extremely simple to extend the RIco program (Navaza, 2003) and FPM (Estrozi and Navaza, 2008) to deal with all rotational point groups. Reconstructions with calculated data have been performed for most symmetries, although the *ab-initio* individual image view

assignment proved to be feasible only for high order symmetry groups when using experimental data.

Acknowledgements

The authors thank Guy Schoehn for providing the DHQ negative stain data and Jon Agirre from the Unidad de Biofísica, UPV (Spain) for boxing the GroEl cryo-em images with his program. J.N. thanks the IKERBASQUE Foundation that made it possible his stay at the Euskal Herriko Unibertsitatea where this work was done.

References

Blanco, M. A., Flórez, M., Bermejo, M., 1997. Evaluation of the rotation matrices in the basis of real spherical harmonics. Journal of Molecular Structure: Theochem 419, 19–27.

Brink, D. M., Satchler, G. R., 1994. Angular Momentum. Oxford University Press, United Kingdom, 3rd revised edition, p. 13–25.

Conway, J. F., Steven, A. C., 1999. Methods for reconstructing density maps of 'single' particles from cryoelectron micrographs to subnanometer resolution. Journal of Structural Biology 128, 106–118.

Estrozi, L. F., Navaza, J., 2008. Fast projection matching for cryo-electron microscopy image reconstruction. Journal of Structural Biology 162, 324–334.

Estrozi, L. F., Navaza, J., 2010. Ab initio high-resolution single-particle 3D reconstructions: The symmetry adapted functions way. Journal of Structural Biology 172, 253–260.

Fan, P.-D., Chen, J.-Q., Draayer, J. P., 1999. Reduced projection operators and algebraic expressions for the symmetry-adapted functions of the icosahedral group. Acta Crystallographica Section A 55, 871–883.

Hanson, R. M., 2010. *Jmol* - a paradigm shift in crystallographic visualization. Journal of Applied Crystallography 43, 1250–1260.

Kovacs, J. A., Wriggers, W., 2002. Fast rotational matching. Acta Crystallographica Section D 58, 1282–1286.

Landau, L. D., Lifschitz, E. M., 1967. Mécanique Quantique. Editions MIR, Moscow, p. 412 and 429.

Liu, H., Cheng, L., Zeng, S., Cai, C., Zhou, Z. H., Yang, Q., 2008. Symmetry-adapted spherical harmonics method for high-resolution 3D single-particle reconstructions. Journal of Structural Biology 161, 64–73.

Navaza, J., 2001. Rotation functions. In: Rossmann, M. G., Arnold, E. (Eds.), Crystallography of Biological Macromolecules. Vol. F of International Tables for Crystallography. International Union of Crystallography, pp. 269–274.

Navaza, J., 2003. On the three-dimensional reconstruction of icosahedral particles. Journal of Structural Biology 144, 13–23.

Prandl, W., Schiebel, P., Wulf, K., 1996. A Recursive Algorithm for the Generation of Symmetry-Adapted Functions: Principles and Applications to the Icosahedral Group. Acta Crystallographica Section A 52, 171–175.

Provencher, S. W., Vogel, R. H., 1988. Three-dimensional reconstruction from electron micrographs of disordered specimens i. method. Ultramicroscopy 25, 209–221.

Schmidt, B., Žďánská, P., 2000. Solution of the time-dependent schrdinger equation for highly symmetric potentials. Computer Physics Communications 127, 290–308.

Trapani, S., Schoehn, G., Navaza, J., Abergel, C., 2010. Macromolecular crystal data phased by negative-stained electron-microscopy reconstructions. Acta Crystallographica Section D 66, 514–521.

Vossman, N., 2008. http://commons.wikimedia.org/wiki/File%3ACryoem_groel.jpg

Zeng, S., Liu, H., Yang, Q., 2010. Application of symmetry adapted function method for three-dimensional reconstruction of octahedral biological macromolecules. International Journal of Biomedical Imaging 2010, Article ID 195274.

Zheng, Y. B., Doerschuk, P. C., 2000. Explicit computation of orthonormal symmetrized harmonics with application to the identity representation of the icosahedral group. SIAM Journal on Mathematical Analysis 32, 538–554.

group	axes orientation		U	W	N	M	K	V	Θ
C_n	n-fold $\parallel \mathbf{Z}$	$\mathcal{P}1$	*as in group* D_n						
		$\mathcal{P}2$	2	0	n	0	-1	–	–
D_n	n-fold $\parallel \mathbf{Z}$, 2-fold $\parallel \mathbf{Y}$		2	0	n	0	1	–	–
T	2-fold $\parallel \mathbf{Z}$, 2-fold $\parallel \mathbf{Y}$	$\mathcal{P}1$	*as in group* O						
		$\mathcal{P}2$	6	2	4	2	1	2	$\pi/2$
O	4-fold $\parallel \mathbf{Z}$, 4-fold $\parallel \mathbf{Y}$		6	2	4	0	1	1	$\pi/2$
I	5-fold $\parallel \mathbf{Z}$, 2-fold $\parallel \mathbf{Y}$ 3-fold in $Y = 0, Z \geq 0$		12	5	5	0	1	1	$\arccos(\sqrt{1/5})$

Table 1: Parameters of the projector formula for rotational point groups.

group	n_ℓ	η	Δ
C_n	$1 + [\ell - (\ell \bmod n)]\, 2/n$	n	2
D_n	$1 + [\ell - n(\ell \bmod 2) - (\ell \bmod n)]\, /n$	$n[1 + (n \bmod 2)]$	$1 + (n \bmod 2)$
T	$1 + [\ell - 3(\ell \bmod 2) - 4(\ell \bmod 3)]\, /6$	6	1
O	$1 + [\ell - 6(\ell \bmod 2) - 4(\ell \bmod 3) - 3(\ell \bmod 4)]\, /12$	12	1
I	$1 + [\ell - 15(\ell \bmod 2) - 10(\ell \bmod 3) - 6(\ell \bmod 5)]\, /30$	30	1

Table 2: Multiplicities and their increments Δ produced by increments η in ℓ .

group	multiplicities
C_n	$n_\ell(\mathcal{P}1) = n_\ell(D_n)$
	$n_\ell(\mathcal{P}2) = n_\ell(\mathcal{P}1) - 1 + 2(\ell \bmod 2)$
T	$n_\ell(\mathcal{P}1) = n_\ell(O)$
	$n_\ell(\mathcal{P}2) = n_\ell(\mathcal{P}1) - 1 + [(\ell \bmod 2) + (\ell \bmod 4)]/2$

Table 3: Number of independent SAFs based on projectors $\mathcal{P}1$ and $\mathcal{P}2$ of groups C_n and T .

group	$\ell_{\max}$	$\max_\ell \left(\frac{\text{max\_eig}_{(\ell)}}{\text{min\_eig}_{(\ell)}}\right) \leq 10\,000$
T	221	9 755
O	224	9 301
I	644	9 346

Table 4: Maximum spherical harmonics degree ℓ for which the ratio between the extreme eigenvalues of the SAF Gramm matrix is smaller than 10 000 .

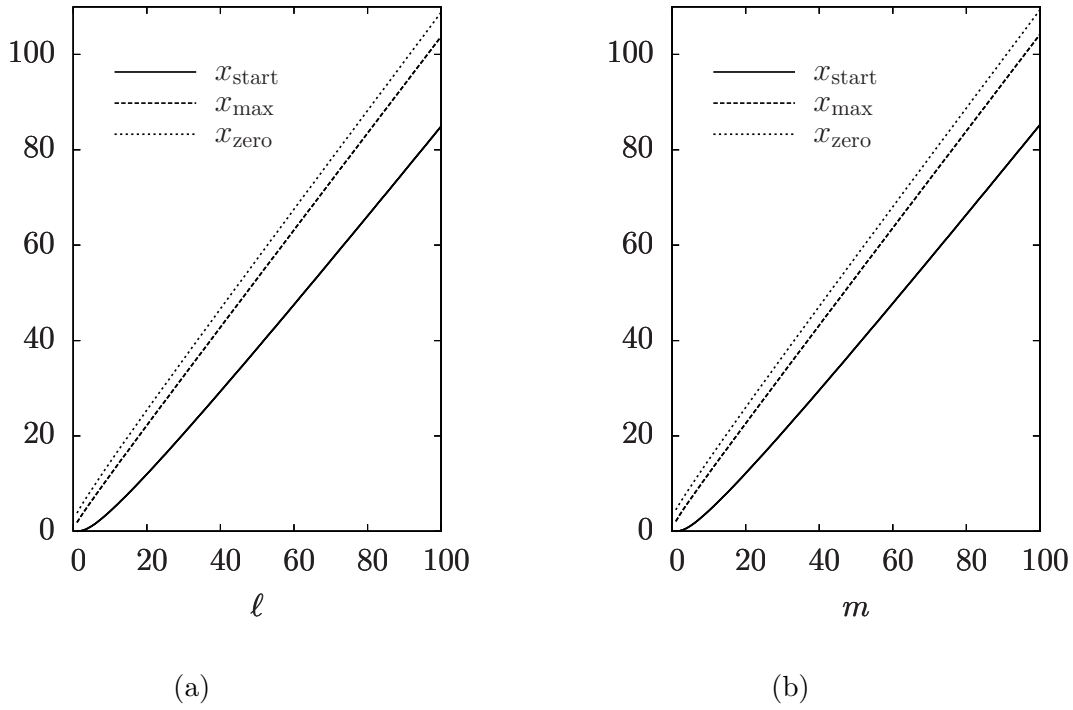

Figure 1: Smallest argument $x_{\rm start}$ at which (a) the Bessel functions $J_m(x)$ and (b) the spherical Bessel functions $j_\ell(x)$ start taking values greater than $10^{-3}\max|J_m|$ and $10^{-3}\max|j_\ell|$, as a function of the orders m and ℓ, respectively. The point of absolute maximum ($x_{\rm max}$) and the first zero ($x_{\rm zero}$) of the functions are also plotted as a function of m and ℓ.

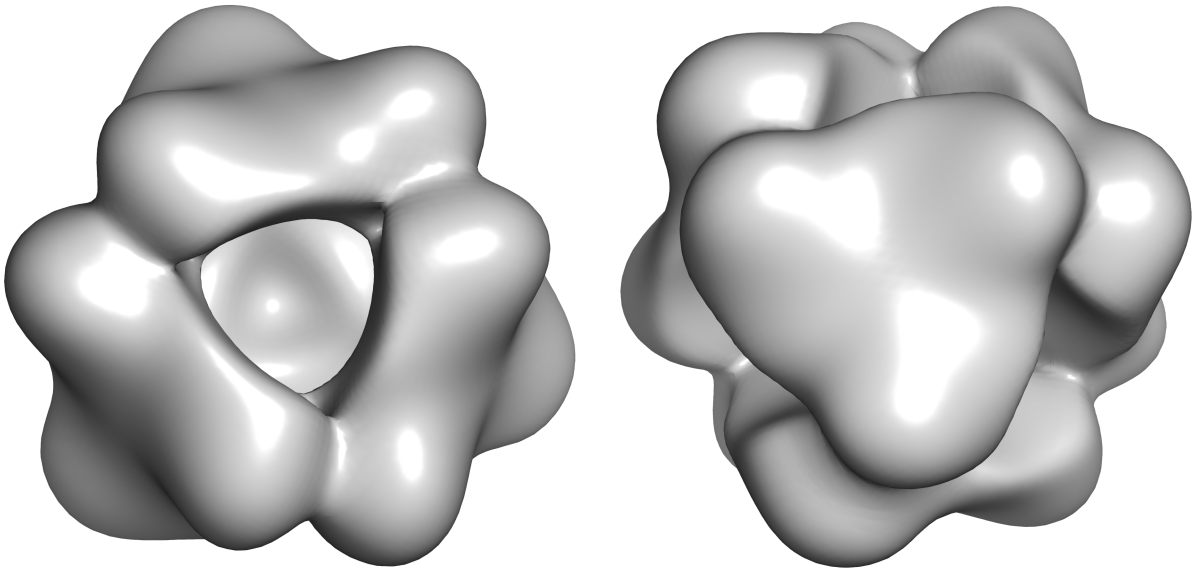

(a)

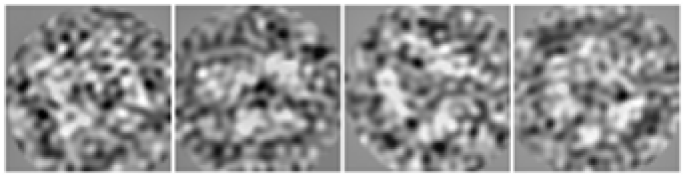

(b)

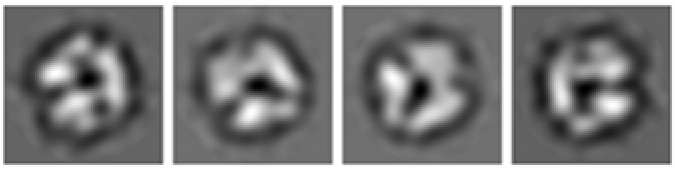

(c)

Figure 2: (a) Two views of the tetrahedral SAF-based TEM reconstruction of DHQ; (b) some of the 2D images used in the reconstruction; (c) projections of the 3D reconstruction along the view directions corresponding to (b).

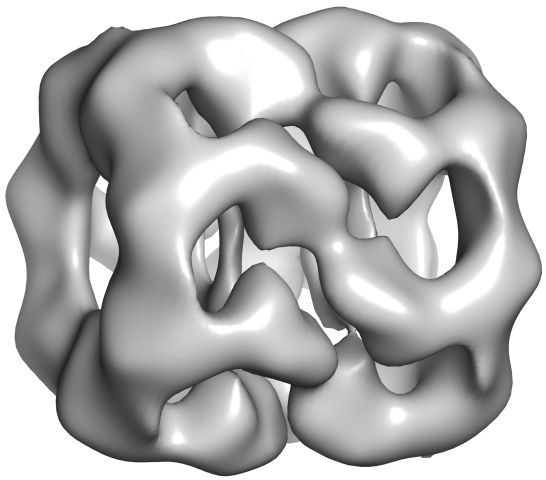

(a)

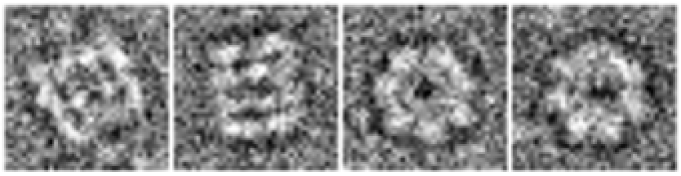

(b)

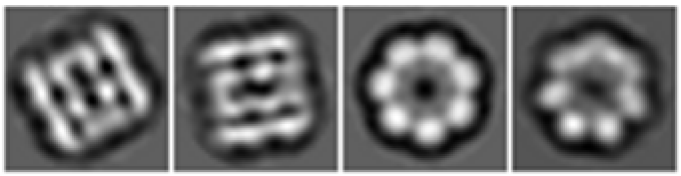

(c)

Figure 3: (a) D_7 SAF-based TEM reconstruction of GroEL; (b) some of the 2D images used in the reconstruction; (c) projections of the 3D reconstruction along the view directions corresponding to (b).